Brodogradnja Volume 75, Number 3 (2024) 75308

journal homepage: www.brodogradnja.fsb.hr

Brodogradnja

An International Journal of Naval Architecture and
Ocean Engineering for Research and Development

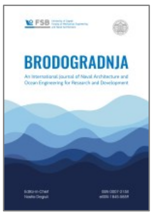

Study on the effect of marine propeller wake on sediment siltation in a shallow water channel

Liu Liang[1*], *Zhang Hao*[2], *Zhang Chaonan*[2], *Chen Jinbiao*[2], *Zhang Baoji*[1], *Bai Xiangen*[2],
Song Shengyao[2], *Chen Qian*[1], *Zhang Weijia*[2]

[1] *College of Ocean Science and Engineering, Shanghai Maritime University, Shanghai, 201306, China*
[2] *Merchant Marine College, Shanghai Maritime University, Shanghai, 201306, China*

ARTICLE INFO

Editor-in-Chief: Prof. Nastia Degiuli
Associate Editor: PhD Ivana Martić

Keywords:
Marine propeller
Wake flow
Unsteady RANS
Channels
Sediment siltation

ABSTRACT

In order to investigate the impact of marine propeller wake fields on sediment siltation in shallow water channels, this study employs the unsteady RANS approach and the Volume of Fluid model. A full-scale numerical self-propulsion test was conducted on a 50,000 DWT oil tanker under the influence of a free surface. The research includes forecasting the effect of propeller wakes on sediment redeposition following the dredging of the approach channel to Jiaxing Port in the China Sea. Initially, uncertainty research was carried out on the full-scale ship and propeller system, and the credibility of the computational results was quantified. The simulated results based on the sediment transport numerical model were then compared and validated against actual data from monitoring stations. The self-propulsion performance and the velocity distribution of the propeller wake were examined under three different propeller speeds. Scenarios simulated included no ship navigation, daily single-ship navigation, and daily two-ship navigation, evaluating the siltation distribution within the channel over one month. The results demonstrate that ship propeller wakes positively influence the reduction of channel sedimentation, with the maximum monthly siltation reduction reaching 0.108 m during single-ship tidal navigation and 0.11 m during two-ship tidal navigation.

1. Introduction

Jiaxing Port in China, authorized by the State Council as a first-class port open to foreign-flagged vessels, boasts superior port construction conditions. However, the Jinshan channel leading into Jiaxing Port is a typical shallow water channel, where the ingress and egress of large vessels are dependent on tidal conditions. This dependency limits the navigational window, necessitating that all large vessels transit at specific tidal levels [1, 2]. As vessels increasingly evolve towards larger sizes, the velocity and influence of ship propeller wake fields also expand. Consequently, the impact of propeller wake fields on sediment resuspension in shallow water channels is an issue that must be considered.

---

[*] Corresponding author.
E-mail address: 3096675628@qq.com

http://dx.doi.org/10.21278/brod75308
Submitted 02 May 2024; Accepted 10 July 2024
ISSN 0007-215X; eISSN 1845-5859

Accurate projections of full-scale vessel performance, as well as dredging and maintenance of port waterways, are critical for ensuring the efficient operation of ships and ports. In the field of ship design and performance assessment, scaled model experiments are commonly used to forecast the propulsion characteristics of full-scale vessels [3, 4]. However, due to variations in Reynolds numbers, scale effects introduce discrepancies between the numerical predictions of model self-propulsion and the actual performance of full-scale ships. To enhance the accuracy of these predictions, it is crucial to employ precise and reliable numerical methods for forecasting the navigational performance of full-scale vessels [5, 6]. Addressing this issue, Milovan Perić [7] conducted a thorough analysis of the treatment of the hull boundary layer and the effects of model scaling. The research indicates that the computational resources required for full-scale numerical simulations do not exceed those for model testing, and the precision of the full-scale calculations is at least equivalent to that of extrapolations using the EFD method. Jang et al. [8], Baltazar et al. [9], and Liang et al. [10] employed an unsteady RANS solver to predict the hydrodynamic characteristics of propellers under various Reynolds numbers in open-water situations. Their research not only meticulously analyzed the scale effects on propellers but also examined the impact of turbulence and transition models on hydrodynamic characteristics predictions. On the other hand, Yao et al. [11, 12] explored the scale effects of propellers from multiple dimensions, including boundary layer flow regimes, frictional and pressure distributions, propeller performance, and tip vortex flows. Their findings indicated that the scale discrepancies in propeller performance primarily originate from different boundary layer flow regimes: the boundary layer flow around real propellers generally exhibits a turbulent state, whereas the blade flow conditions of model propellers are more intricate and highly correlated with the Reynolds numbers. Feng et al. [13], Kok et al. [14], and Yu et al. [15] employed the body force method as a propulsion model for numerical simulations of self-propulsion performance at both model and full scales for a KCS container ship. Sun et al. [16, 17] utilized the RANS method and VOF model to conduct numerical simulations of the interactions between the model-scale and full-scale vessel with the free surface. The results they obtained showed a good agreement between the numerical analysis of the self-propulsion traits of full-sized vessels, taking into account their roughness and free surface impacts, and the data from sea trials. Mikkelsen et al. [18] integrated a roughness model directly into the numerical calculation of self-propulsion for ro-ro and general cargo ships at full scale using modified wall function methods, comparing these with sea speed trial measurements. They found that incorporating the roughness model directly into CFD calculation provided more precision than using traditional empirical formulas derived from towing tank extrapolations. Jasak [19] and Saydam [20] applied the unsteady RANS method to compute the self-propulsion performance at both model and full scales for a small product tanker and a bulk carrier, along with a mesh sensitivity study. Comparative sea trials on the target ships further substantiated the reliance on the unsteady RANS method in forecasting self-propulsion characteristics.

Concurrently, to ensure the smooth arrival of vessels at ports, numerous scholars have conducted extensive research on the phenomenon of channel siltation at ports, employing methods such as field observations and laboratory physical model experiments [21]. Berends et al. [22] developed a high-fidelity composite method that effectively quantifies the total siltation and its spatial distribution uncertainties in approach channels, significantly reducing computational costs compared to traditional direct Monte Carlo simulations. Li et al. [23, 24] utilized the Mike 21 FM simulation tool to analyze sediment movements in channels near ports and predicted the siltation conditions, aiming to implement appropriate measures under extreme weather conditions to prevent sediment accumulation and ensure normal vessel navigation and port operations. Lee and his research group [25], focusing on Incheon North Port in Korea, used adjusted hydrographic and dredging data to estimate sedimentation rates and further explored the dominant mechanisms of channel resiltation.

During navigation, ship propeller jets induce disturbances in the water body, leading to the erosion, transport, and resuspension of sediment from the bed surface. Currently, there are few research cases focusing on the influence of ship propeller jets on channel sediment redeposition. However, in certain specific channels, the effects of ship propeller wake fields on sediment redeposition need to be considered. Through physical model tests, the influence of ship propeller wake on sedimentation can be simulated under laboratory conditions. This method provides intuitive observational data and phenomena; however, it is very costly and time-consuming. Therefore, this study employs the CFD software STAR-CCM+ in conjunction with MIKE21 for the research. First, based on the unsteady RANS method, the VOF model is used to capture the free surface, and a full-scale self-propulsion numerical simulation is conducted for a 50,000 DWT oil tanker. A sediment transport numerical model is established using MIKE21 and validated against observational data from monitoring stations. To verify the engineering reliability of the CFD method, numerical simulations of open-water propeller performance and hull resistance were conducted. The self-propulsion characteristics and the velocity distribution of the propeller wake at three different propeller speeds are obtained. By simulating the sediment deposition evolution within the channel over a month for three navigation scenarios, this study discusses the impact of propeller wake fields on sediment redeposition in the approach channel to Jiaxing Port in the open sea under varying densities of ship traffic.

2. Computational method and numerical modeling

2.1 Geometry

In this paper, a 50000DWT oil tanker is taken as the research object, and the three-dimensional geometric model of the hull, rudder, and propeller is established according to the type line drawings and data provided by the ship owner as shown in Figs. 1 and 2, and the parameters of the ship model are shown in Table 1.

Table 1 Geometrical particulars of 50,000 Oil Tankers.

	Project	Value
Hull	Overall length, L_{OA} (m)	183.00
	Length between perpendiculars, L_{PP} (m)	174.00
	Breadth, B (m)	32.20
	Depth, D_H (m)	19.10
	Structural draft (m)	13.60
	Design draft, d (m)	11.0
	Displacement (m^3)	60000
Rudder	Rudder area, A_R (m^2)	42.26
	Rudder fore area (m^2)	13.986
	Rudder aft area (m^2)	28.274
	Balance ratio (%)	67
	Aspect ratio	1.685
	Rudder height, H (m)	9.17
Propeller	Diameter D_P (m)	6.80
	No. of blades	4
	Angle of skew (°)	18.21
	Angle of rake (°)	0
	Pitch ratio, P/D_P	0.852
	Disk ratio, A_E/A_O	0.422
	Direction of rotation	Right-hand

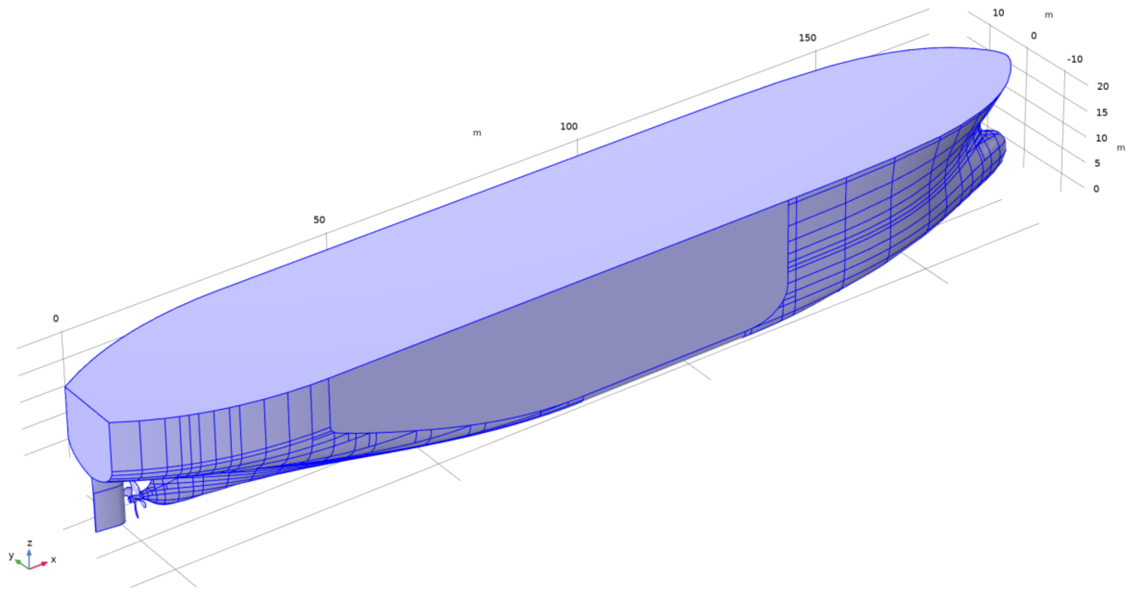

Fig. 1 Geometrical model of 50000DWT oil tanker

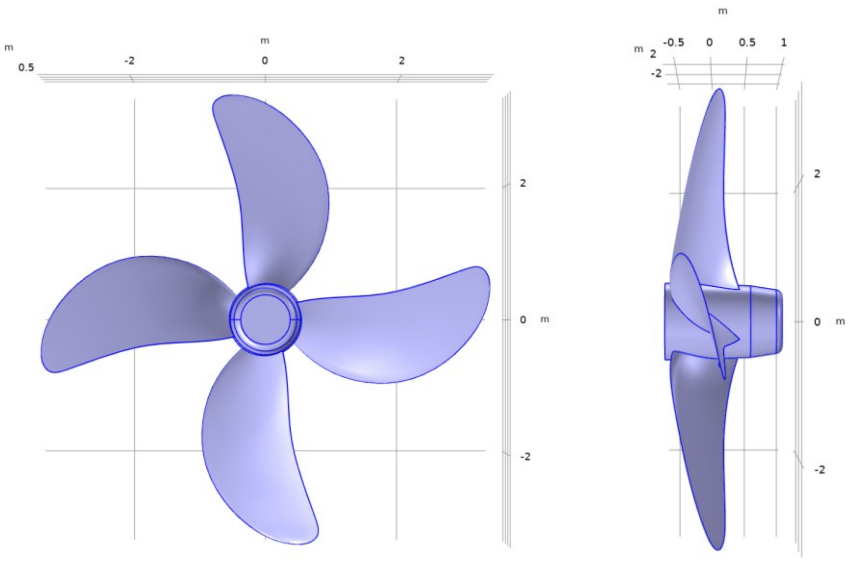

Fig. 2 Geometrical model of the propeller for a 50000DWT oil tanker

2.2 Fluid model

In numerical calculations of full-scale vessel self-propulsion tests, the fluid surrounding the hull and propeller is considered to be incompressible and viscous. According to the hypothesis, the winding flow field around the vessel may be solved using the Reynolds-averaged Navier-Stokes equations. The equations in Cartesian coordinates are as follows:

$$\frac{\partial U_i}{\partial x_i} = 0 \tag{1}$$

$$\frac{\partial U_i}{\partial t} + \frac{\partial U_i U_j}{\partial x_j} = -\frac{1}{\rho}\frac{\partial P}{\partial x_i} + \frac{1}{\rho}\frac{\partial}{\partial x_j}\left(\mu \frac{\partial U_i}{\partial x_j} - \rho \overline{u_i' u_j'}\right) \tag{2}$$

where U_i and u_i' are mean and fluctuating Cartesian velocity components $(i, j = 1, 2, 3)$; ρ, p, μ, f_i, and $\rho\overline{u_i'u_j'}$ are the fluid density, the time-averaged value of pressure, dynamic viscosity coefficient of fluid, mass force, and Reynolds stress term, respectively.

This study employs a rectangular computational domain to assess the propulsion characteristics of full-sized ships, with the flow field computational domain illustrated in Fig. 3. In the body-fixed coordinate system, the external flow field dimensions are: $-3.5L_{PP} < X < 2.5L_{PP}$, $-2.0L_{PP} < Y < 2.0L_{PP}$, $-1.5L_{PP} < Z < 1.0L_{PP}$. The area surrounding the propeller is encapsulated by a cylindrical domain to form a rotating region, with dimensions: $-0.4D_P < X < 0.2D_P$, Rotating=$1.2D_P$. The simulation of the propeller's rotation is described using a multi-slip mesh approach. Regarding boundary conditions, the interface between the rotating and external computational domains is handled using an interface boundary, where data is transferred between the internal and external flow fields. The hull and propeller surfaces are designated as no-slip wall boundaries, the flow field domain outlet is set as a pressure outlet, and all remaining external boundaries are configured as velocity inlets. Damping is added at the outlet and side boundaries to prevent wave reflection.

During the simulation process, the VOF method is employed to solve for the free surface. The VOF function can be defined as:

$$\frac{\partial C}{\partial t} + u\frac{\partial C}{\partial x} + v\frac{\partial C}{\partial y} = 0 \tag{3}$$

When C =0, the mesh is full of subphase fluid; when C =1, the mesh is full of main-phase fluid; and when $0 < C < 1$, the mesh containing the fluid interface becomes an interfacial mesh.

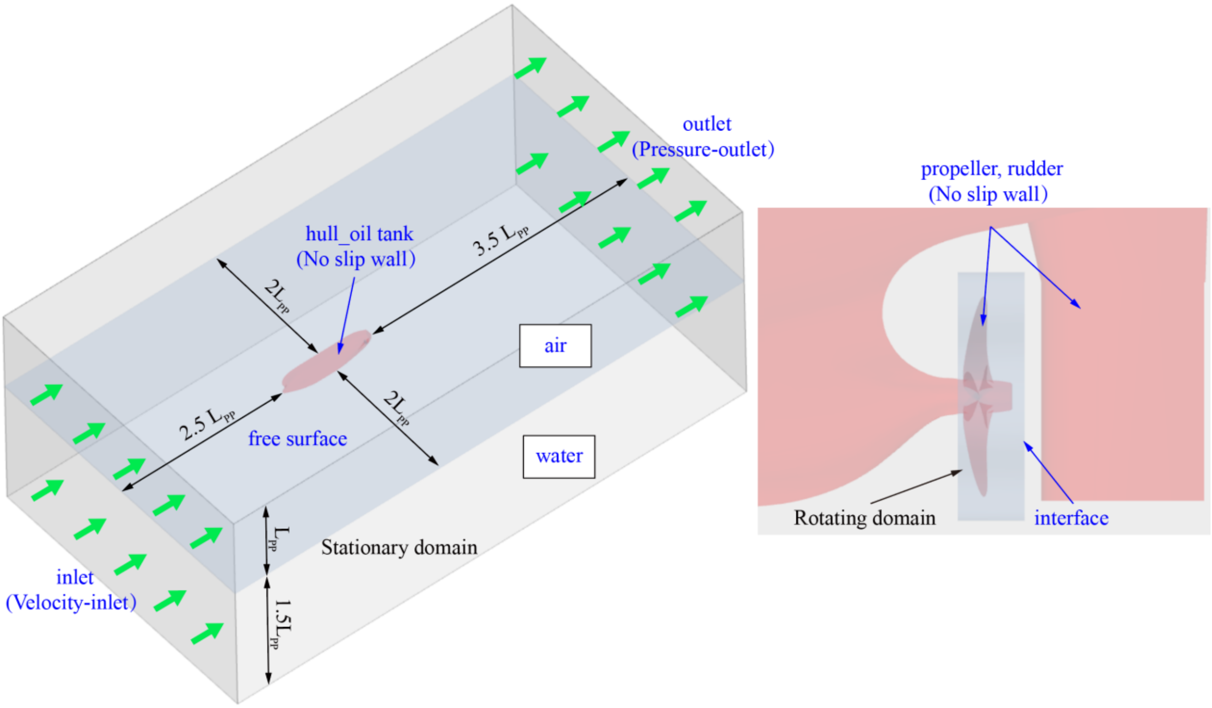

Fig. 3 The computational domain used for solving the self-propulsion performance of ships

In the computational region of the flow field, an unstructured hexahedral mesh is employed for discretization, as depicted in Fig. 4. To better capture the waveform of the free surface, a denser mesh is used near the hull and waterline areas. Additionally, the grid is refined around the bow, stern, and rudder areas to enhance the accuracy of the flow field analysis. The details of the mesh near the hull and propeller are shown in Fig. 5. Prism-shaped grids are utilized near the surfaces of the hull and its appendages to more effectively resolve the near-wall flow. In the numerical simulation of the full-scale ship self-propulsion, the k-Epsilon turbulence model is applied to solve the flow in the near-wall regions.

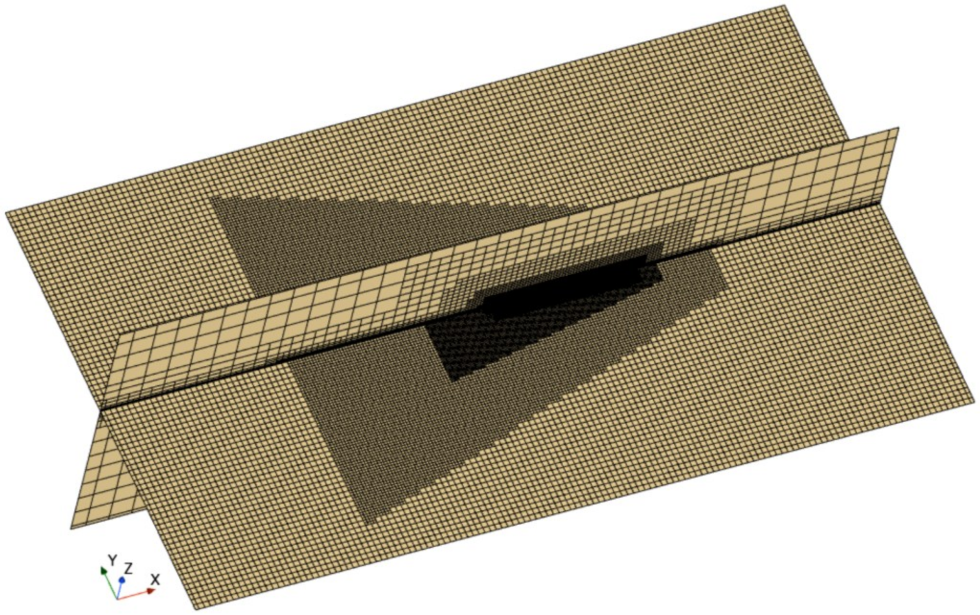

Fig. 4 Fluid domain computational grid

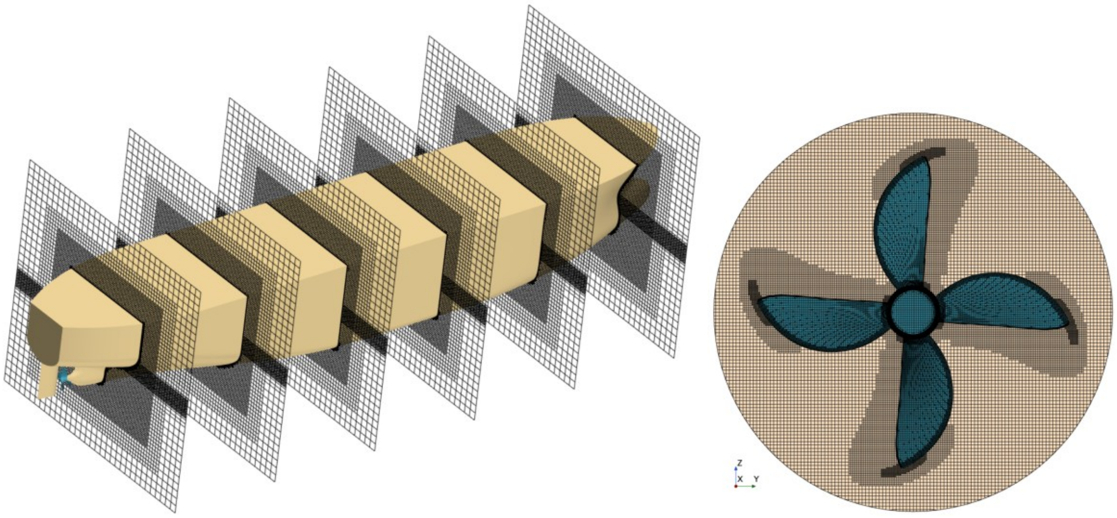

Fig. 5 The grid details in the region near the hull and propeller

In this study, the Two-Layer All *y*+ Wall Treatment is used to handle the near-wall region flow. This approach is designed to effectively manage a wide range of *y*+ values. The Two-Layer All *y*+ Wall Treatment combines two main wall treatment methods. When the mesh is sufficiently fine, with the first layer of grid cells located within the viscous sublayer (typically $y+ < 5$), a no-wall-function approach is used to directly calculate the flow near the wall. For coarser meshes, where the first layer of grid cells is located in the logarithmic layer (typically $y+ > 30$), wall functions are used to describe the near-wall region flow. The *y*+ distributions on the hull and propeller surfaces are shown in Fig. 6.

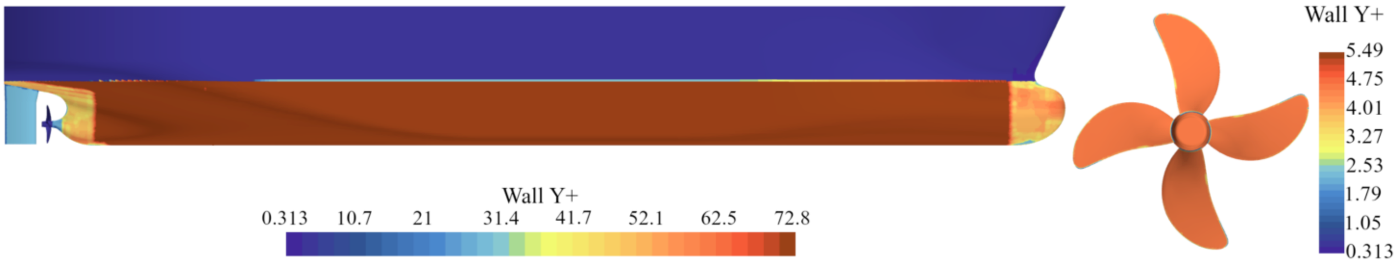

Fig. 6 *y*+ distribution on the wall

2.3 Study area

The study area is located in the approach channel to Jiaxing Port off the coast of China, which is an artificial navigation trench primarily used for the temporary mooring of vessels, as depicted in Fig. 7. As the principal access channel to Jiaxing Port, the Jinshan channel features generally shallow waters. Therefore, large vessels must fully capitalize on tidal conditions for port entry, necessitating specific navigational window restrictions that require ships to navigate according to tidal movements.

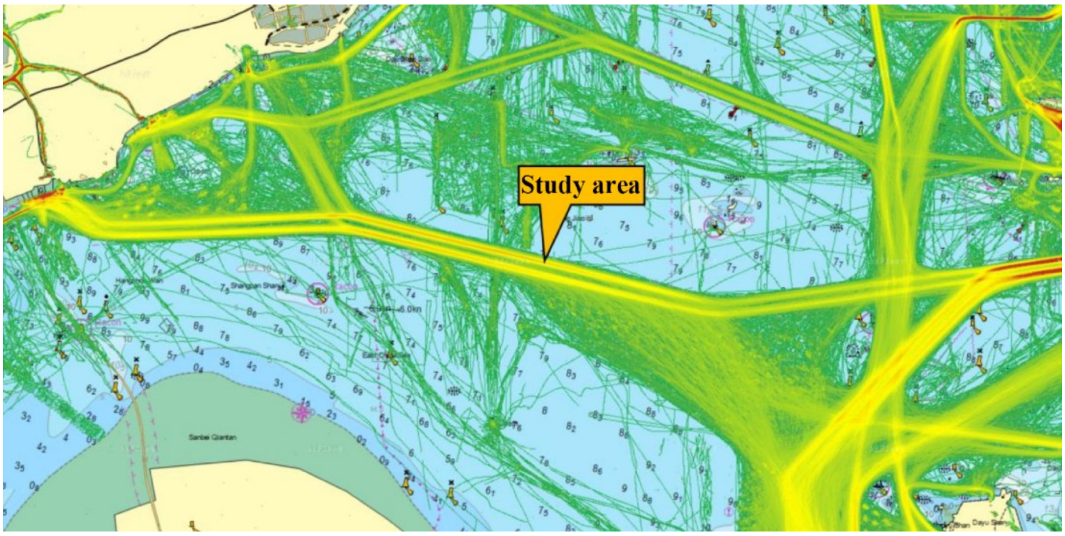

Fig. 7 AIS trajectory map of the study area

The artificial navigation channel under study is 1500 meters long and 250 meters wide, with a designed bottom elevation of -11.5 meters. The lateral slopes range from 1:5 to 1:10, while the longitudinal slope is 1:50. According to local navigational authorities, the maximum allowed speed within this channel is 10 knots. The coordinates for the simulation area are 639920 m < X < 646279 m, and 3378619 m < Y < 3382095 m, based on the 1954 Beijing coordinate system with a Gauss-Krüger projection and a central meridian at 120°. This study utilizes an unstructured grid to discretize the computational domain and employs grid refinement in the area of the artificial channel. Bathymetric data from nautical charts are imported into the model and interpolated to generate a terrain cloud map. The location and bathymetric distribution of the artificial channel are shown in Fig. 8.

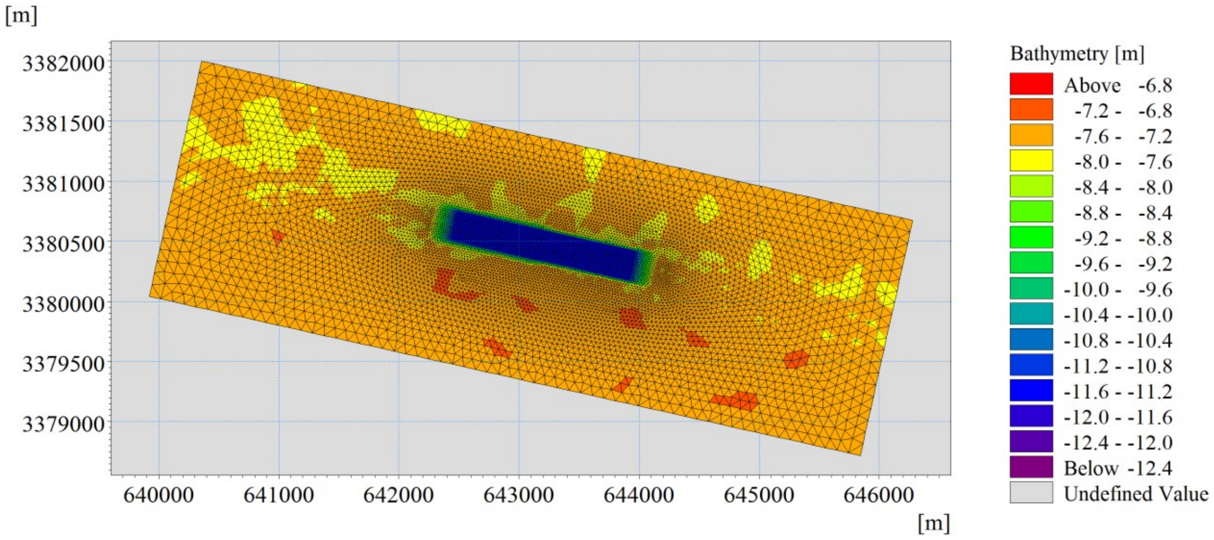

Fig. 8 Location and water depth distribution of artificial navigation channels

2.4 Sediment transport model

MIKE 21 is capable of handling a wide range of hydrodynamic, material transport and ecological models for a wide range of applications in the simulation and analysis of river, lake, coastal and marine environments. MIKE 21 has been developed by the Danish Hydraulic Institute (DHI). The movement of cohesive sediments in the MIKE21 MT model is described by the advection-diffusion equation, which can be expressed as:

$$\frac{\partial \overline{c}}{\partial t}+u\frac{\partial \overline{c}}{\partial x}+v\frac{\partial \overline{c}}{\partial y}=\frac{1}{h}\frac{\partial}{\partial x}\left(hD_x\frac{\partial \overline{c}}{\partial x}\right)+\frac{1}{h}\frac{\partial}{\partial y}\left(hD_y\frac{\partial \overline{c}}{\partial y}\right)+Q_LC_L\frac{1}{h}-S \tag{4}$$

In the equation: u and v represent the depth-averaged flow velocities in the horizontal direction (m/s), c represents the depth-averaged sediment concentration (kg/m³), h represents the water depth, S is the point source term, obtained from CFD calculations (kg/m³/s), D_x and D_y represent the diffusion coefficients in the x and y directions, respectively.

In MIKE 21 MT module, the hydrodynamic effects are typically described using bottom shear stress, which is divided into two main types: pure current action and combined wave-current action. According to hydrological data provided by the Jiaxing Port Authority, the study area is a shallow water region where wave action can be neglected. Therefore, this study is conducted under pure current action.

$$\tau_c=\frac{1}{2}\rho f_c V^2 \tag{5}$$

where

$$f_c=2\left(2.5\left(\ln\left(\frac{30h}{k}\right)-1\right)\right)^{-2} \tag{6}$$

In the equation, τ_c represents the bottom shear stress, V represents the average flow velocity under pure tidal current conditions, f_c represents the friction factor under tidal current conditions, ρ represents the fluid density, k represents the seabed roughness.

3. Verification and Validation

3.1 Numerical uncertainty analysis

Before conducting full-scale numerical self-propulsion simulations of ships, this study initially verified and validated the computational methods used to ensure accuracy and efficiency in the calculations. Specifically, detailed verification and validation studies were carried out on the full-sized models of both the propeller and the hull.

Numerical uncertainty U_{SN} is composed of grid uncertainty U_G, time step uncertainty U_T, iterative uncertainty U_I, and uncertainty in other parameters U_P, which can be defined as follows:

$$U_{SN}^2=U_G^2+U_T^2+U_I^2+U_P^2 \tag{7}$$

Building on previous research [26,27], this paper posits that compared to grid uncertainty U_G and timestep uncertainty U_T, the uncertainties associated with iterations U_I and other parameters U_P are negligible. Consequently, this study focuses on convergence analysis for grids and timesteps as a means to estimate uncertainty.

In the study of uncertainty, this paper conducts an in-depth analysis of the thrust and torque of a propeller as well as the total resistance of a 50,000 DWT oil tanker. The Richardson extrapolation method is employed for a systematic analysis of grid spacing and timestep intervals. Specifically, Δx_1, Δx_2, and Δx_3 represent the grid or timestep intervals for the fine, medium, and coarse grids, respectively. The uniform parameter refinement ratio ri can be expressed as:

$$r_i = \frac{\Delta x_1}{\Delta x_2} = \frac{\Delta x_2}{\Delta x_3} \tag{8}$$

Correspondingly, C_1, C_2, and C_3 are the computed results for the fine, medium, and coarse grids. The convergence factor R is defined as:

$$R = \frac{\varepsilon_{21}}{\varepsilon_{32}} = \frac{C_2 - C_1}{C_3 - C_2} \tag{9}$$

Three cases of convergence can be determined based on the R-value:

(1) $0 < R < 1$; Monotonic convergence:

(2) $R < 0$; Oscillatory convergence:

(3) $R > 1$; divergence:

When monotonic convergence is achieved, Richardson's extrapolation method can be used. The estimated numerical error δ_{RE} and the accuracy level P_{RE} can be calculated according to the following equations.

$$\delta_{RE} = \frac{\varepsilon_{21}}{r_i^{P_{RE}} - 1} \tag{10}$$

$$P_{RE} = \frac{\ln(\varepsilon_{32}/\varepsilon_{21})}{\ln r_i} \tag{11}$$

The calibration coefficient C_g is defined as:

$$C_g = \frac{r_i P_{RE} - 1}{r_i P_{TH} - 1} \tag{12}$$

where P_{TH} is an estimate of the limiting order of the computational accuracy when the interval tends to zero; typically, $P_{TH} = 2$. The numerical error δ_{SN}, the benchmark result $C_{R,}$ and the uncertainty $U_{G,T}$ can be estimated as:

$$\delta_{SN} = C_g \delta_{RE} \tag{13}$$

$$C_R = C - \delta_{SN} \tag{14}$$

$$U_{G,T} = \begin{cases} \left(9.6\left(1 - C_g\right)^2 + 1.1\right)\left|\delta_{RE}\right|, & \left|1 - C_g\right| < 0.125 \\ \left(2\left|1 - C_g\right| + 1\right)\left|\delta_{RE}\right|, & \left|1 - C_g\right| \geq 0.125 \end{cases} \tag{15}$$

Figs. 9 and 10 respectively illustrate three different grid conditions for the full-scale blade and hull grid uncertainty studies. In these figures, variations in surface mesh density, and the number of mesh layers are observed among the fine, medium, and coarse mesh, with a mesh refinement ratio set at $\sqrt{2}$. The hull utilizes an identical segmentation strategy, resulting in a mesh refinement ratio of $\sqrt[3]{2}$.

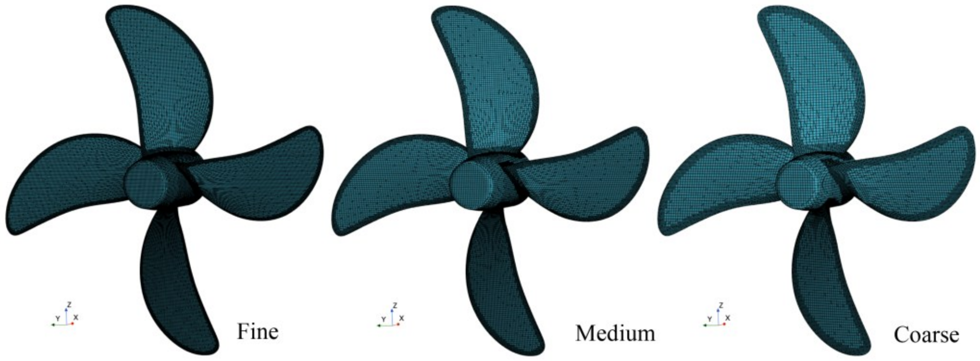

Fig. 9 Three mesh strategies for Full-Scale propellers

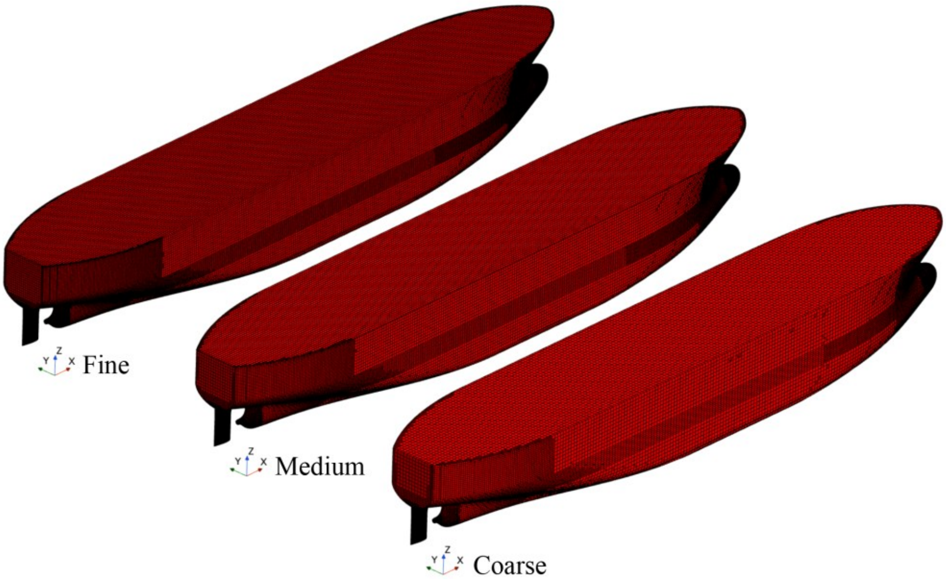

Fig. 10 Three mesh strategies for Full-Scale hulls

Table 2 Results of full-scale for the different mesh.

Grid	propeller					hull		
	Cell (M)	K_T	Error %	K_Q	Error %	Cell (M)	C_t (10^{-3})	Error %
Coarse	3.67	0.1571	-5.418	0.0225	-4.255	7.64	2.285	4.961
Medium	6.82	0.1644	-1.023	0.0231	-1.702	10.51	2.22	1.975
Fine	12.31	0.1654	-0.421	0.02341	-0.383	16.42	2.1791	0.096
EFD	—	0.1661	—	0.0235	—	—	2.177	—

For the numerical uncertainty analysis, operating conditions $J = 0.6$ for the propeller and $Fn = 0.154$ for the hull are chosen. Regarding the sensitivity research of timestep intervals, a midpoint timestep of 2 degrees per time step for the propeller and a midpoint timestep of $0.0025L_{PP}/V_m$ for the hull, where Vm represents the ship's speed, with a refinement ratio of 2 for both cases, are chosen. The simulation results for the full-scale propeller and hull of a 50,000DWT oil tanker using different mesh and time-step intervals are presented in Tables 2 and 3, respectively. The mesh uncertainty research is based on the midpoint timestep. For the analysis of mesh distance and timestep intervals, the convergence factor R is within the range of 0 to 1, indicating monotonic convergence and enabling the use of the Richardson extrapolation method. As shown in Table 4, the uncertainties in propeller thrust are 3.015%D and 0.807%D, while those for torque are 3.837%D and 2.263%D, where D represents the data from experiments. The hull's sensitivities stand at 4.723%D and

0.574%*D*. The results indicate that the propeller thrust and torque, as well as the hull resistance, are sensitive to the grid spacing.

Table 3 Results of full-scale for the different time steps.

Time step	propeller					hull		
	Δt (s)	K_T	Error %	K_Q	Error %	Δt (s)	C_t (10^{-3})	Error %
Coarse	0.008	0.1549	-6.743	0.022	-6.383	0.096	2.31	6.109
Medium	0.004	0.1644	-1.023	0.0231	-1.702	0.068	2.22	1.975
Fine	0.002	0.1655	-0.361	0.0234	-0.426	0.048	2.175	-0.092
EFD	—	0.1661	—	0.0235	—	—	2.177	—

Table 4 Results of uncertainties analysis.

			r_i	R	C_g	$U_{G,T}$ (%D)	U_{SN} (%D)
Propeller	K_T	Grid (G)	$\sqrt{2}$	0.137	6.304	3.051	3.156
		Time step (T)	2	0.116	2.545	0.807	
	K_Q	Grid (G)	$\sqrt{2}$	0.517	0.936	3.837	4.455
		Time step (T)	2	0.273	0.889	2.263	
Hull	C_t	Grid (G)	$\sqrt[3]{2}$	0.629	1.003	4.723	4.758
		Time step (T)	$\sqrt{2}$	0.500	1.001	0.574	

The difference between the water tank experimental data D and the numerical results S is defined as the comparative error E. In full-scale numerical simulations, D represents the extrapolated value of the model's Empirical Fluid Dynamics (EFD) data [28].

$$E = D - S \tag{16}$$

The validation uncertainty U_V can be expressed as:

$$U_V^2 = U_D^2 + U_{SN}^2 \tag{17}$$

Table 5 provides the results of the validation study, where U_D, representing the uncertainty of the experimental data, is set at 1.00%D. According to the results of the validation study, all values of E are less than those of U_V, thus validating the computational results in aspect U_V.

Table 5 Results of the validation study.

		U_{SN} (%D)	U_D (%D)	U_V (%D)	E (%D)
Propeller	K_T	3.156	1	3.311	1.023
	K_Q	4.455	1	4.566	1.702
Hull	C_t	4.758	1	4.862	1.975

3.2 Development and validation of a mathematical model for cohesive sediment

This study utilizes the MIKE 21 MT module to construct a sediment transport model, which comprises one sediment layering group and two-bed layers. Specifically, the first bed layer is a soft mud layer, and the second bed layer is a hard mud layer. To verify the accuracy of the model, observed sediment concentration data from locations C1 (coordinates *X*=640521.8118 m, *Y*=3381201.1832 m) and C2 (coordinates *X*=645806.0143 m, Y=3379561.979 m) were compared with numerical simulation results, as illustrated in

Figs. 11 and 12. The simulation spanned from 19:00 on August 21, 2021, to 04:00 on August 23, 2021. Solid lines in the graphs represent the simulation outcomes, while the scatter points indicate observed data. The graphs display trends in sediment concentration over time, and the alignment between the simulated and observed data is remarkably high, with a relative error in sediment concentration of less than 5%. These results demonstrate that the sediment transport model established in this study is highly accurate and capable of effectively predicting sediment dynamics in the entrance channel of Jiaxing Port.

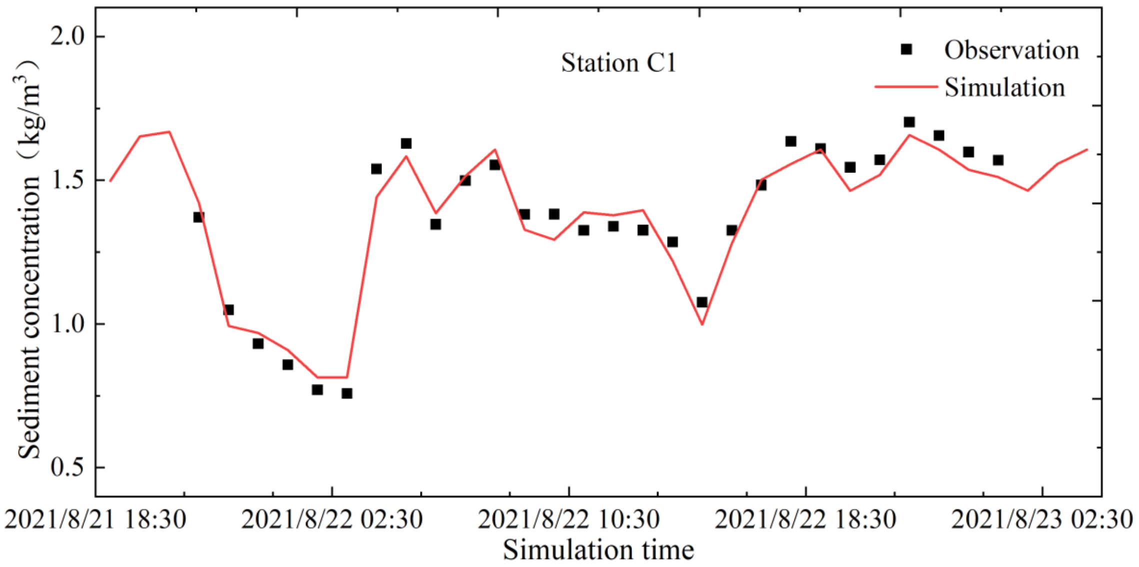

Fig. 11 Verification of sediment concentration at Station C1.

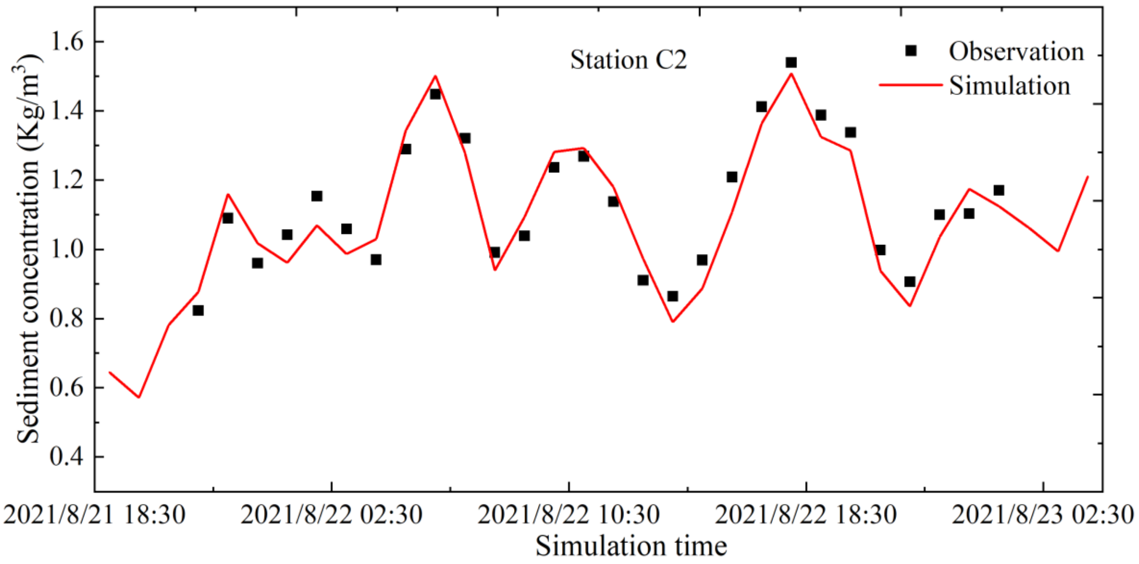

Fig. 12 Verification of sediment concentration at Station C2.

4. Results and discussion

4.1 Numerical prediction of full-scale open water and resistance performance.

The hydrodynamic characteristics of marine propellers are expressed by three dimensionless coefficients: the thrust coefficient K_T, the torque coefficient K_Q, and the efficiency η_0. These coefficients are defined as follows:

$$J = \frac{V_A}{Dn} \tag{18}$$

$$K_{TM} = \frac{T_M}{\rho n^2 D_P^4} \tag{19}$$

$$K_{QM} = \frac{Q_M}{\rho n^2 D_P^5} \tag{20}$$

$$\eta_0 = \frac{J}{2\pi} \bullet \frac{K_{TM}}{K_{QM}} \tag{21}$$

where: T, Q, ρ, n, V_A and J are the thrust, torque, density, rotation speed, advance velocity, and advance coefficient, respectively.

The hydrodynamic characteristics of full-scale propellers can be calculated based on the characteristics of the model propellers.

$$K_{TS} = K_{TM} - \Delta K_T \tag{22}$$

$$K_{QS} = K_{QM} - \Delta K_Q \tag{23}$$

where:

$$\Delta K_T = -\Delta C_D \cdot 0.3 \cdot \frac{P}{D} \cdot \frac{c \cdot Z}{D} \tag{23}$$

$$\Delta K_Q = \Delta C_D \cdot 0.25 \cdot \frac{c \cdot Z}{D} \tag{24}$$

The difference in drag coefficient C_D can be expressed as

$$\Delta C_D = C_{DM} - C_{DS} \tag{25}$$

where:

$$C_{DM} = 2\left(1 + 2\frac{t}{c}\right)\left[\frac{0.044}{(Re_{0.7})^{\frac{1}{6}}} - \frac{5}{(Re_{c0})^{\frac{2}{3}}}\right] \tag{26}$$

and

$$C_{DS} = 2\left(1 + 2\frac{t}{c}\right)\left(1.89 + 1.62 \cdot \log\frac{c}{k_{\mathrm{p}}}\right)^{-2.5} \tag{27}$$

In the formula, c is the chord length, t is the maximum thickness, P/D is the pitch ratio, $Re_{0.7}$ is the local Reynolds number. k_{p} represents the blade roughness.

This article predicts the open-water characteristic of a full-scale propeller across an advanced ratio range of J=0 to J=0.85. The propeller operates at a constant rotational speed, and variations in the advance coefficient J are achieved by adjusting the inflow velocity V_A. The open water performance of the full-scale propeller, as shown in Fig. 13, is compared with tank test data provided by KRISO. The relative error for the thrust coefficient K_T is less than 1.02%, and for the torque coefficient K_Q, it is less than 2.62%. Therefore, the numerical simulation results obtained by the CFD method for full-scale propellers can meet the requirements of engineering applications. The CFD method is valuable for accurately predicting the open-water performance of marine propellers.

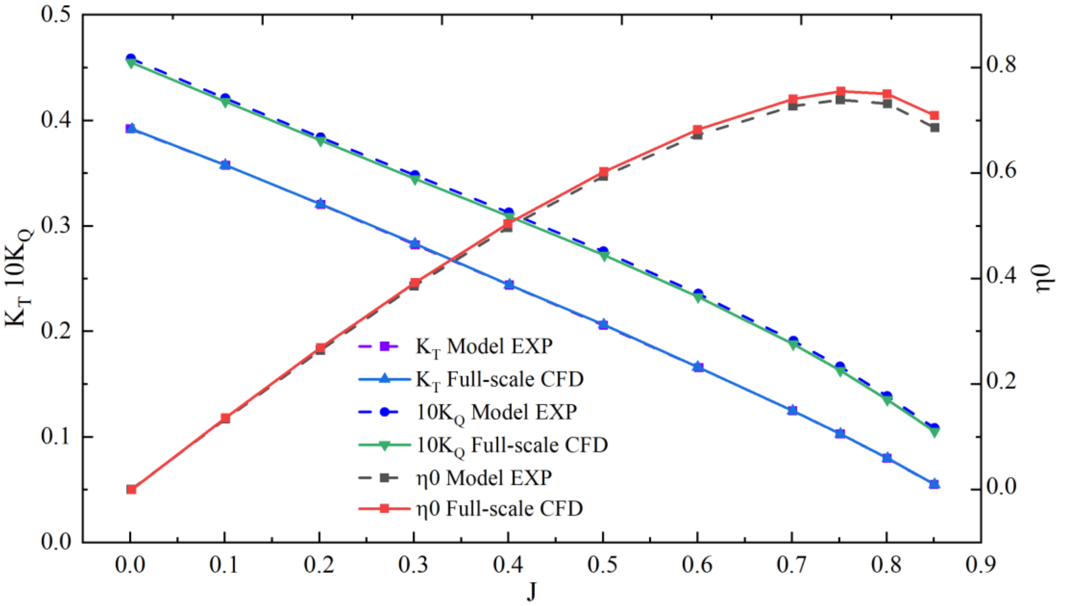

Fig. 13 Open water performance curve of the Full-Scale propeller for a 50,000 DWT oil tanker.

KRISO conducted bare-hull resistance experiments on a 50,000 DWT oil tanker using a model scale of 1:27.2 and extrapolated the model test resistance data to the full-scale ship using the method provided by ITTC-1978 [29].

Total resistance coefficient of model is:

$$C_{TM} = \frac{R_{TM}}{\frac{1}{2}\rho S_m {V_m}^2} \tag{28}$$

Wave resistance coefficient is:

$$C_W = C_{TM} - (1+k)C_{FM} \tag{29}$$

where Frictional resistance coefficient C_{FM} can be expresses as:

$$C_{FM} = \frac{0.075}{(log_{10}^{Re} - 2)^2} \tag{30}$$

Then, the total resistance coefficient of full scale ship is

$$C_{TS} = (1+k)C_{FS} + \Delta C_F + C_W + C_A + C_{AAS} \tag{31}$$

where k is the form factor, C_{FS} is the frictional resistance coefficient of the ship, ΔC_F is the roughness allowance, which can be expressed as:

$$\Delta C_F = 0.044\left[\left(\frac{k_s}{L_{WL}}\right)^{\frac{1}{3}} - 10\cdot \mathrm{Re}^{-\frac{1}{3}}\right] + 0.000125 \tag{32}$$

where k_s indicates the roughness of hull surface.

C_A is the correlation allowance, which can be expressed as:

$$C_A = (5.68 - 0.6\log\mathrm{Re})\times 10^{-3} \tag{33}$$

C_{AAS} is the air resistance coefficient, which can be expressed as:

$$C_{AAS} = C_{DA}\frac{\rho_A \cdot A_{VS}}{\rho \cdot S_S} \tag{34}$$

where A_{VS} is the projected area of the ship above the water line to the transverse plane, S_S is the wetted surface area of the ship, ρ_A is the air density, and C_{DA} is the air drag coefficient of the ship above the water line.

CFD was employed to predict the bare-hull resistance of the full-scale vessel at speeds of 12, 13, 14, and 15 knots. The effective power obtained from CFD simulations was compared with experimental values, as illustrated in Fig. 14. The comparison shows that the experimental data and CFD simulation results are in excellent agreement, with a maximum relative error of no more than 5%. This further demonstrates the feasibility of applying CFD methods to the self-propulsion numerical simulations of full-scale ships.

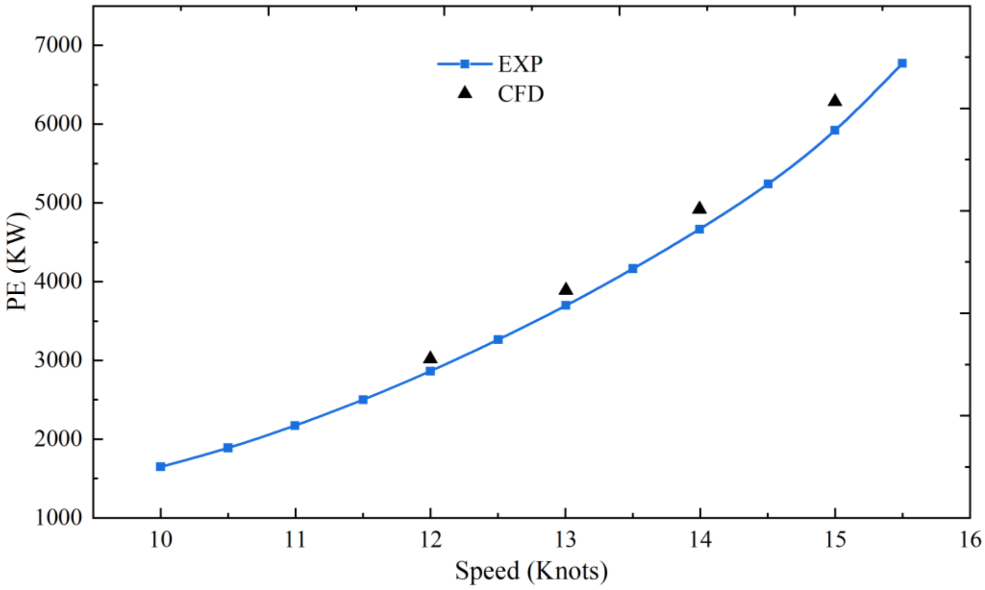

Fig. 14 Effective power comparison for a 50,000 DWT oil tanker

4.2 Numerical calculation of full-scale self-propulsion working condition

The medium grid was chosen for the self-propulsion numerical simulation of the full-scale ship, with a mesh count of 16 million. The reason for selecting the medium grid is that it ensures a certain level of accuracy while improving computational speed and saving computational resources. The numerical simulation of a full-scale ship's self-propulsion trial does not require friction resistance adjustments due to variations in Reynolds numbers. The propeller's operating conditions, including its rotational speed, thrust, and torque, are determined when the hull resistance and propeller thrust balance each other. This effectively avoids errors introduced by resistance conversion and scale effects of wake flow. Based on the propeller rotational speeds and ship speeds obtained from full-scale sea trials, the propeller's rotational speed for a specified service speed is estimated through interpolation. The estimated self-propulsion point rotational speed of the propeller is $N0$=68 RPM. Two additional rotational speeds, $N1$=66 RPM and $N2$=70 RPM, are selected within a suitable range around $N0$. Subsequently, numerical simulations are performed for these three different propeller rotational speeds at a service speed of V=10 knots (d=11.0 m). The curves illustrating the variation of hull resistance and propeller thrust with propeller speed are plotted, and the intersection of these curves determines the self-propulsion point at this speed.

Through full-scale self-propulsion numerical simulations, the propeller thrust, torque, and hull resistance were calculated for three different propeller rotational speeds, as shown in Table 6. The full-scale self-propulsion trial curve is depicted in Fig. 15. By interpolating where the resistance R_S equals the propeller thrust T_S, the self-propulsion point N is determined to be 67.752 RPM, with $R_S = T_S = 437202.678$ N. In this study, the sliding mesh method was employed to capture the transient effects of the propeller. This method was chosen because accurately simulating the propeller wake is crucial for understanding its impact on channel sedimentation. Although the MRF method offers high computational efficiency, it cannot capture transient effects and is insufficiently accurate for simulating the propeller's transient effects. Figs. 16 and 17 show the vortex structures of the propeller wake field captured using the sliding mesh method and the MRF method, respectively, at service speed. Compared to the MRF method, the unsteady RANS method combined with sliding mesh technology can more intuitively and accurately present the wake velocity distribution, flow characteristics, and vortex structures of the propeller.

Table 6 Numerical simulation results of real ship self-propelled at different rotational speeds

N (RPM)	R_S (N)	T_S (N)	Q_S (Nm)
66	432000	400710	342100
68	438000	441800	373900
70	443800	484700	406800

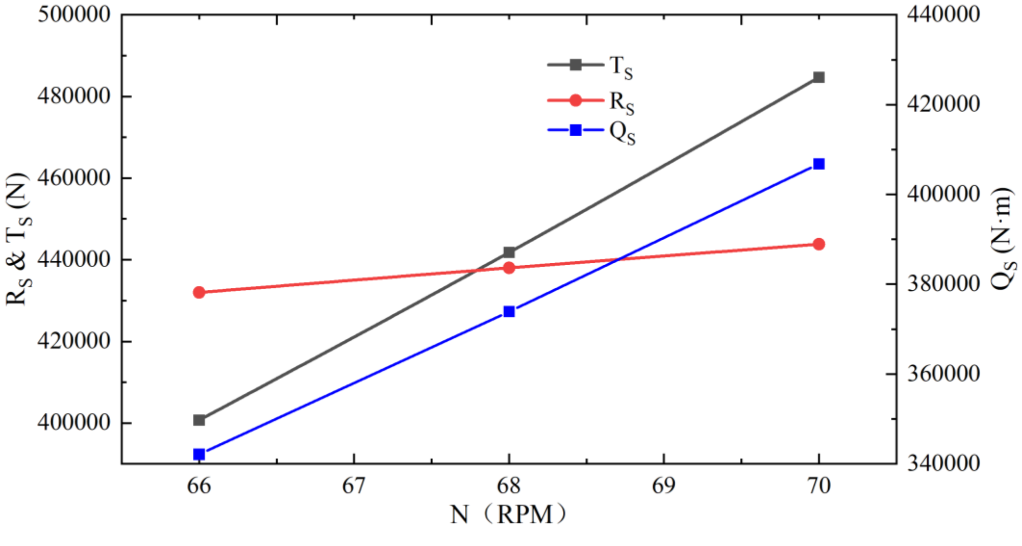

Fig. 15 Full-Scale ship Self-Propulsion test curves

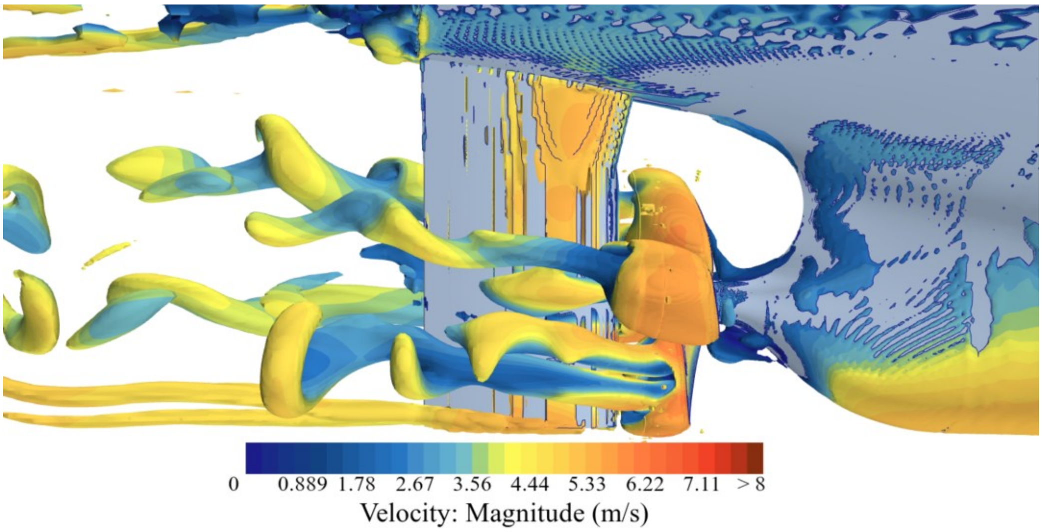

Fig. 16 The vortex structures captured by the MRF method

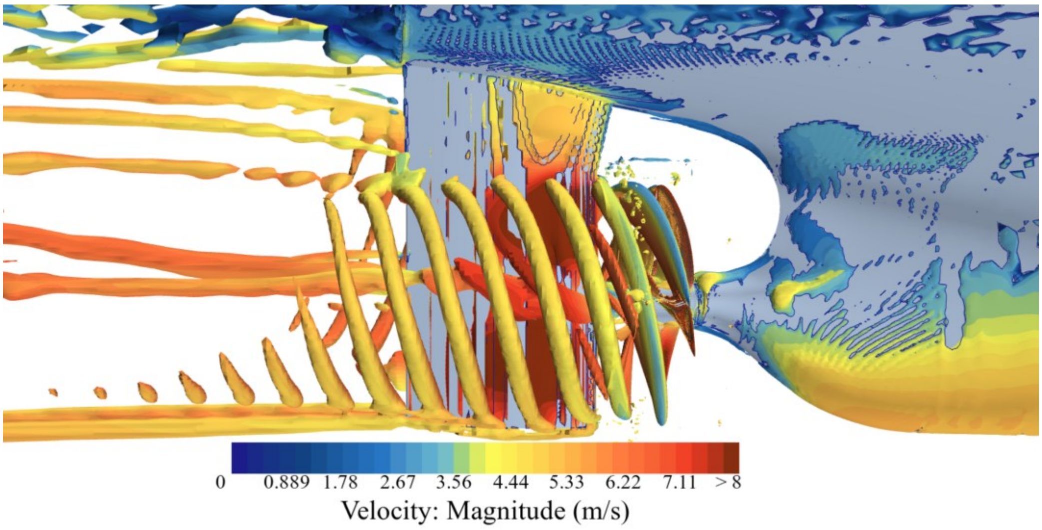

Fig. 17 Predicting vortex structures around propellers and rudders based on the Q-Criterion

4.3 Numerical Simulation of Channel Siltation Intensity.

In the study area, four cross-sections—SC1, SC2, SC3, and SC4—were selected along the transverse direction, beginning at the eastern slope of the navigation channel and spaced 500 meters apart. Vertically, given the navigation channel's width of 250 meters, selecting only one section might lead to significant errors in calculating the longitudinal siltation intensity. Therefore, in this study, three longitudinal sections—L1, L2, and L3—were chosen. The L1 section is located at the central position of the navigation channel, L2 on the north side of the center, and L3 on the south side. The distance between sections L2 and L3 and the central section L1 is 75 meters. The detailed section locations are shown in Fig. 18.

A numerical simulation of sediment movement was conducted for a 50,000-ton artificial navigation channel, resulting in the depiction of siltation evolution within the channel over the month from June 1, 2024, to July 1, 2024. The longitudinal distribution of seabed heights and siltation thickness changes along the artificial channel are illustrated in Fig. 19. The figure shows that along the channel's length, the siltation depths at sections L1, L2, and L3 initially decrease and then increase, a trend attributable to the presence of channel slopes. At the eastern and western ends of the channel, the siltation depth at section L1 is notably higher than at the other two longitudinal sections, while in the central area of the channel, section L1 shows slightly less siltation than the other sections. Along the channel, the maximum siltation depth is 0.23 meters, with the minimum in the central area being 0.012 meters. The distribution of seabed heights and changes in siltation thickness in both longitudinal and transverse sections of the artificial channel are shown in Fig. 20. Across the channel's width, siltation depth increases from south to north at sections SC1 and SC4, while it decreases at sections SC2 and SC3. The maximum siltation depth across the channel is 0.39 meters.

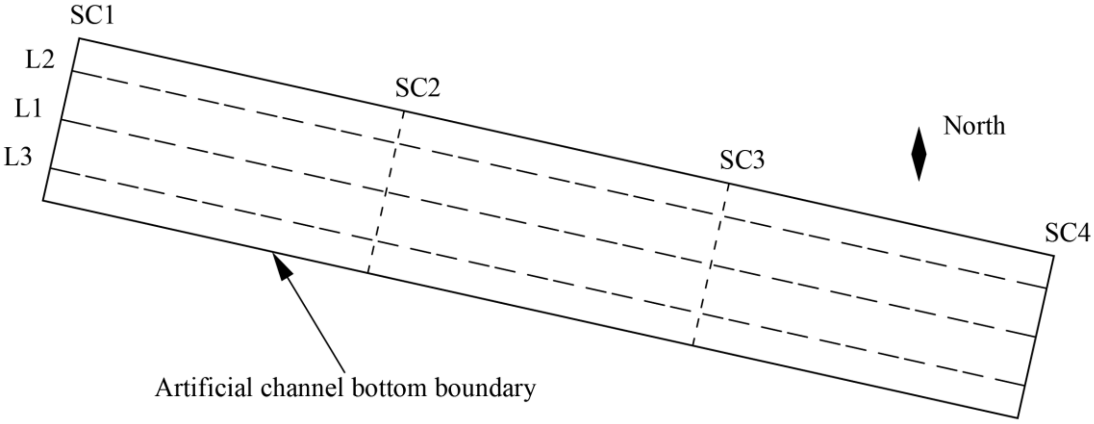

Fig. 18 Calculated section position in the artificial navigation channel

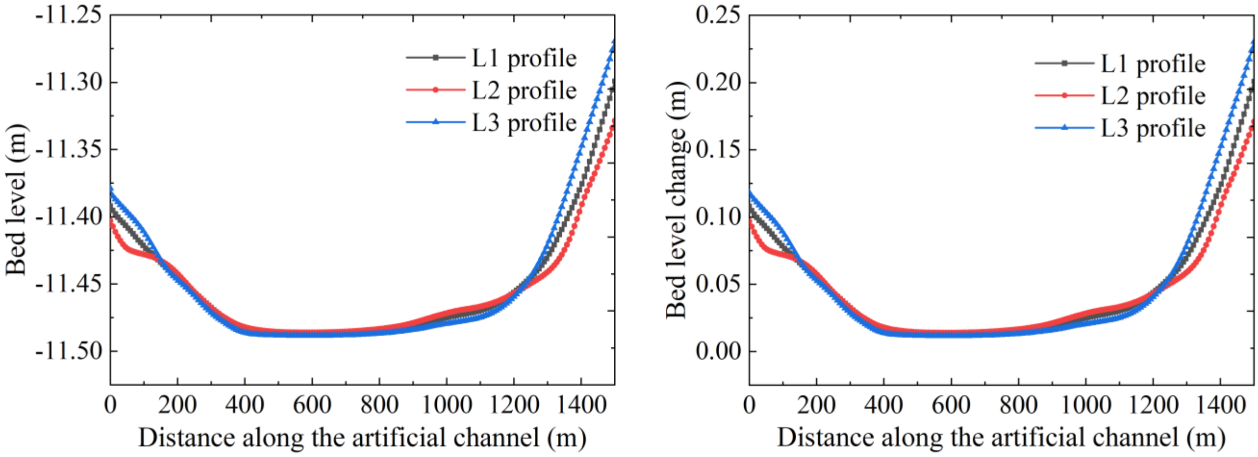

Fig. 19 Longitudinal distribution of seabed elevations and sediment thickness in an artificial navigation channel

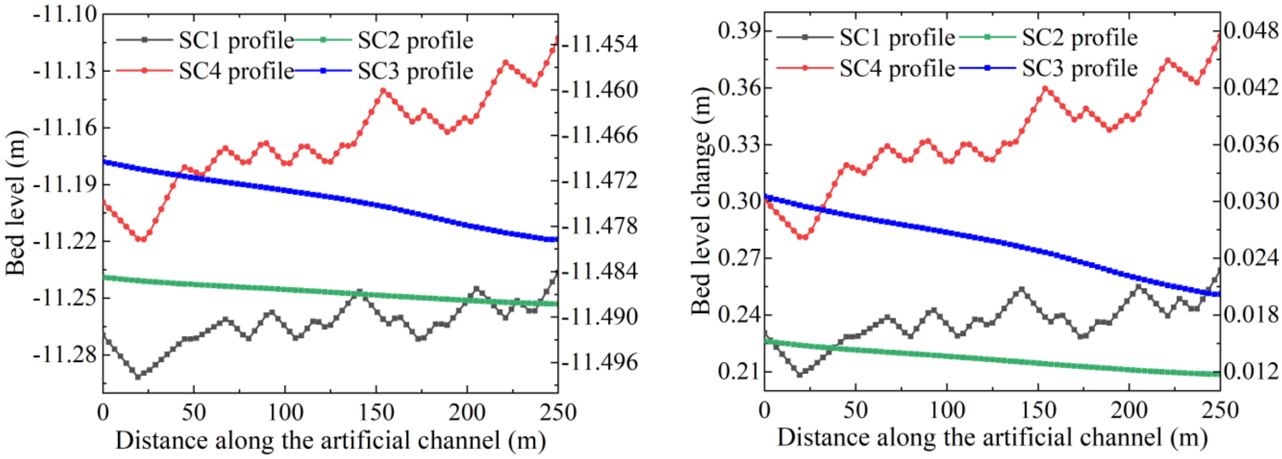

Fig. 20 Transverse distribution of seabed elevations and sediment thickness in an artificial navigation channel

4.4 The Influence of Propeller Wake Fields on Channel Siltation.

The velocity field of the propeller wake was extracted from the self-propulsion numerical results and applied as a point source in the artificial channel in MIKE21, as shown in Fig. 21. Under different navigation densities, the duration of the point source effect varies, but the source strength remains constant. The higher the navigation density, the longer the duration of the point source effect.

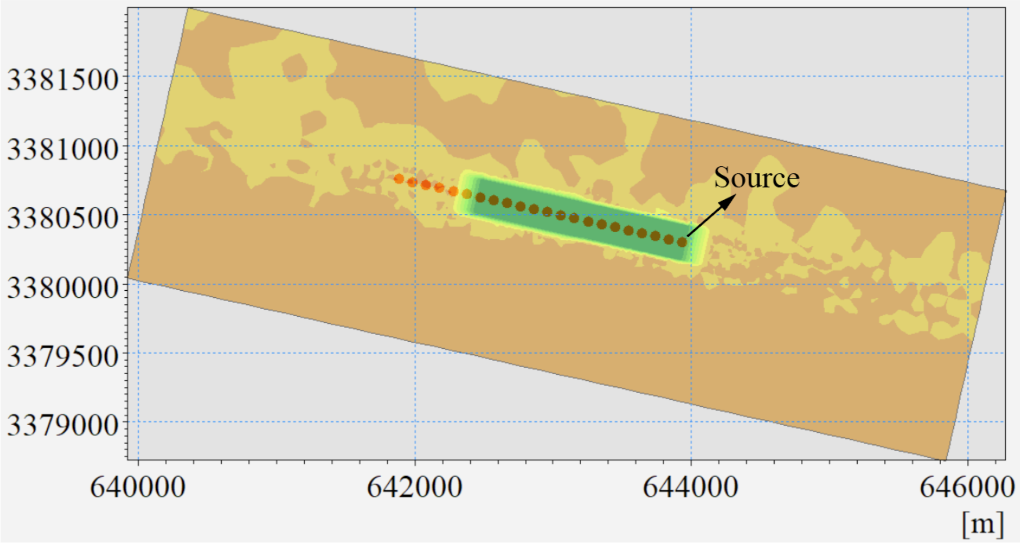

Fig. 21 Distribution of source

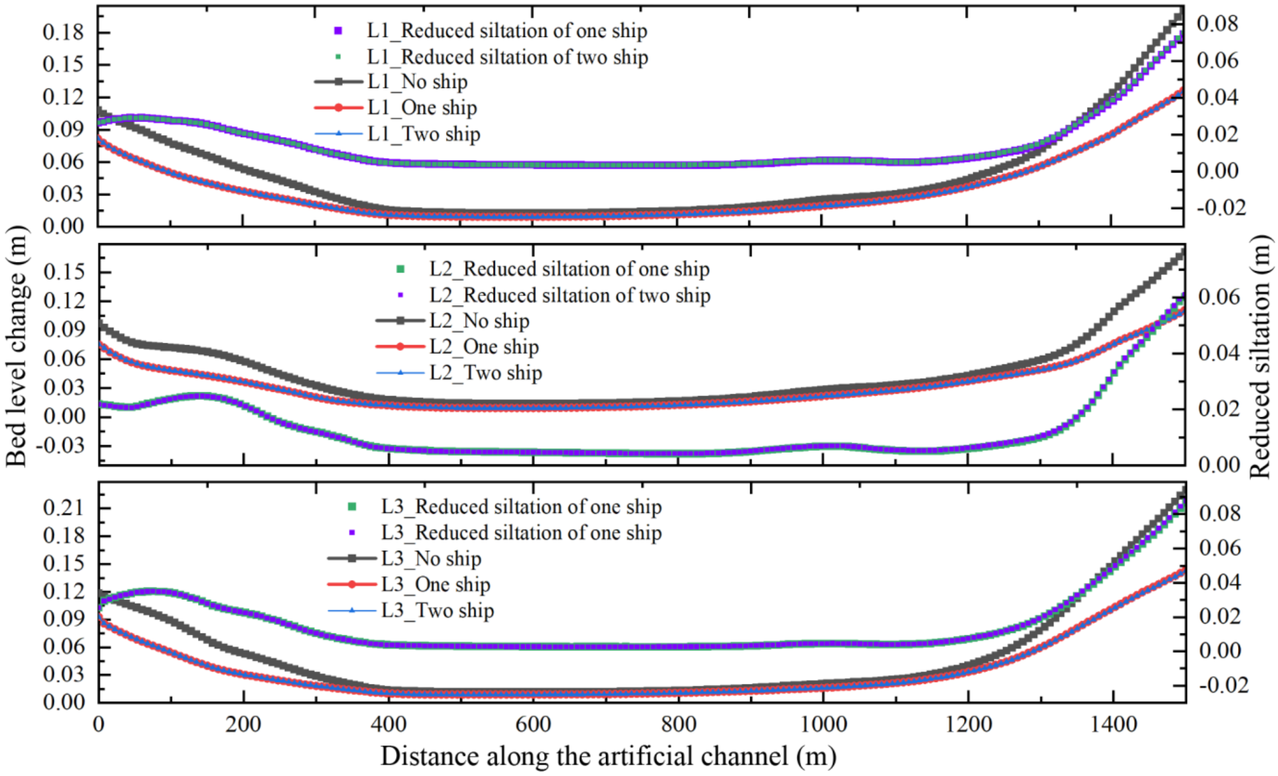

Fig. 22 Comparison of monthly desilting volumes in longitudinal profiles under different navigational densities

To investigate the impact of ship propeller wakes on channel siltation under different navigation densities, this paper compares the effects of ship wakes on channel siltation between daily single-ship tidal navigation and daily double-ship tidal navigation, with simulations running from June 1, 2024, to July 1, 2024. Along the length of the channel, the comparison of siltation reduction effects at various sections over one month is shown in Fig. 22. Due to the higher siltation depths at the eastern and western sides of the channel compared to the central part, the siltation reduction effects at the three longitudinal sections are significantly greater on the sides than in the middle. Across the width of the channel, the comparison of siltation reduction effects at various sections over one month is depicted in Fig. 23. For sections, SC1 and SC4, the northern side shows better siltation reduction due to higher siltation depths in the northern part of the channel compared to the southern part. Conversely, for sections SC2 and SC3, the southern side shows better siltation reduction due to higher siltation depths in the southern part of the channel compared to the northern part. It is evident that ship navigation and the consequent propeller wakes play a positive role in reducing channel siltation. The maximum monthly siltation reduction during daily single-ship tidal navigation is 0.108 meters, and it increases slightly to 0.11 meters during daily double-ship tidal navigation.

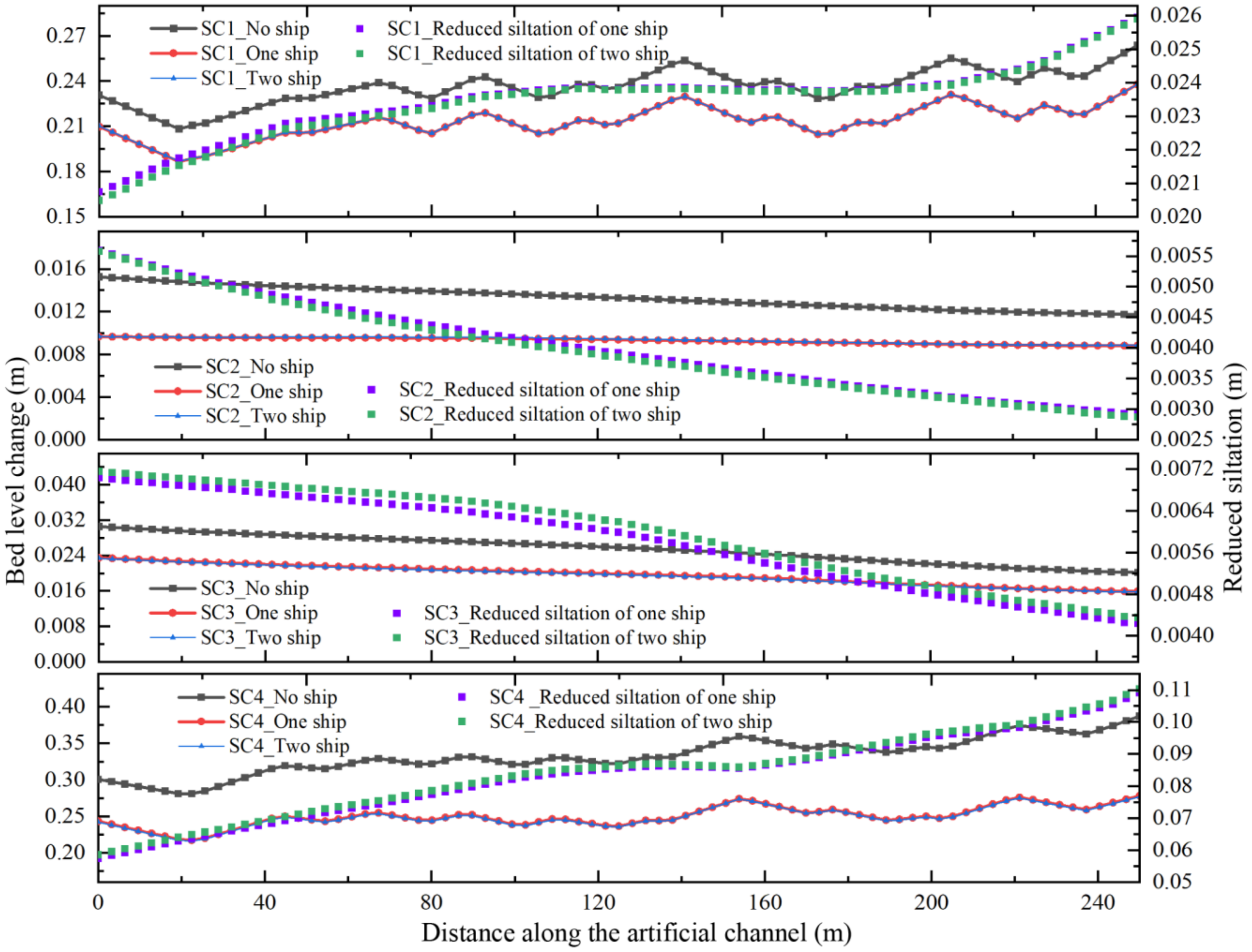

Fig. 23 Comparison of monthly desilting volumes in transverse profiles under different navigational densities

5. Conclusion

This paper presents a full-scale self-propulsion numerical simulation of a 50,000 DWT oil tanker using the unsteady RANS method. A sediment transport numerical model was established using MIKE21 and validated through comparison with observational data from monitoring stations. The simulation addressed the open-water performance of the propeller and the hull resistance to discuss scale effects. By simulating the sedimentation evolution within the channel over a month under three different navigation scenarios, the study explores the impact of propeller wake fields on sediment resuspension in the approach channel to Jiaxing Port under varying ship navigation densities. The study reaches the following conclusions:

1. The CFD calculations of the full-scale propeller's thrust coefficient K_T and torque coefficient K_Q show relative errors of less than 1.02% and 2.05%, respectively, compared to the tank test data provided by KRISO. This indicates that the numerical simulation results obtained by the CFD method for full-scale propellers can meet the requirements of engineering applications.

2. The effective power of the full-scale vessel predicted by the CFD method, compared to extrapolated experimental data, exhibits relative errors that increase with ship speed, with the maximum error not exceeding

5%. Because extrapolation from model-scale to full-scale experiments is not precise. The comparison shows the difference between the two predictions, which are both affected by different sources of error. This also confirms the reliability of using the CFD method for full-scale self-propulsion numerical simulations.

3. Comparisons with observed sediment concentrations at monitoring stations verify the accuracy of the sediment transport model developed in this study, capable of predicting future sediment dynamics in the artificial navigation channel leading to Jiaxing Port. Longitudinally along the channel, the siltation depth over a month shows an initial increase followed by a decrease. Transversely across the channel, the siltation depth in the SC1 and SC4 sections increases from south to north, while the siltation depth in the SC2 and SC3 sections gradually decreases. The maximum siltation depth in the entire channel is 0.39 meters, and the minimum siltation depth is 0.012 meters.

4. By comparing the impact of propeller wake on channel siltation under different navigation densities, it can be observed that the propeller wake of ships has a very positive effect on reducing siltation in shallow waterways. Longitudinally along the channel, the desilting effect is significantly higher on the east and west sides compared to the center of the channel. Transversely across the channel, the desilting effect is better on the north side than on the south side for the SC1 and SC4 sections, while the desilting effect is better on the south side than on the north side for the SC2 and SC3 sections. For the entire channel, the maximum monthly desilting volume is 0.108 meters for one ship navigating with the tide per day, and 0.11 meters for two ships navigating with the tide per day.

ACKNOWLEDGEMENT

The authors gratefully acknowledge the support from the Shanghai Municipal Science and Technology Commission Local College Capacity Building Project (Z20228005), National Natural Science Foundation of China (Grant Nos. 51779135 and 51009087) and Shanghai Natural Science Foundation of China (project approval number: 14ZR1419500).

REFERENCES

[1] Qiang, L., Bing-Dong, Y., Bi-Guang, H., 2018. Calculation and measurement of tide height for the navigation of ship at high tide using artificial neural network. *Polish Maritime Research*, 25(s3), 99-110. https://doi.org/10.2478/pomr-2018-0118

[2] Noshokaty, S. E., 2023. Shipping optimisation systems for liner: en-route bunkering, port late arrival, and tide restricted sailing. *International Journal of Shipping and Transport Logistics*, 16(1-2), 154-169. https://doi.org/10.1504/IJSTL.2023.128573

[3] Wang, C., Sun, S., Li, L., Ye, L., 2016. Numerical prediction analysis of propeller bearing force for full-scale hull–propeller–rudder system. *International Journal of Naval Architecture and Ocean Engineering*, 8(6), 589-601. https://doi.org/10.1016/j.ijnaoe.2016.06.003

[4] Dai, K., Li, Y., Gong, J., Fu, Z., Li, A., Zhang, D., 2022. Numerical study on propulsive factors in regular head and oblique waves. *Brodogradnja*, 73(1), 37-56. https://doi.org/10.21278/brod73103

[5] Visonneau, M., 2005. A step towards the numerical simulation of viscous flows around ships at full scale-Recent achievements within the European Union Project Effort. *Royal Institute of Naval Architecture Marine CFD*, Southampton, France.

[6] Li, L., Wang, C., Sun, S., Sun, S., 2016. Numerical simulation and scale effect of self-propulsion test of a full-scale ship. *Journal of Harbin Engineering University*, 37(7), 901-907. https://doi.org/10.11990/jheu.201507015

[7] Perić, M., 2019. Full-scale simulation for marine design. Siemens PLM Software. Available from: https://www.plm.automation.siemens.com/global/en/resource/full-scale-cfd/85998.

[8] Jang, Y.-H., Eom, M.-J., Paik, K.-J., Kim, S.-H., Song, G. 2020. A numerical study on the open water performance of a propeller with sinusoidal pitch motion. *Brodogradnja*, 71(1), 71-83. https://doi.org/10.21278/brod71105

[9] Baltazar, J., Rijpkema, D., Falcão De Campos, J., 2021. Prediction of the propeller performance at different Reynolds number regimes with RANS. *Journal of Marine Science and Engineering*, 9(10), 1115. https://doi.org/10.3390/jmse9101115

[10] Liang, L., Baoji, Z., Hao, Z., Hailin, T., Weijie, W., 2023. Hydrodynamic performance optimization of marine propellers based on fluid-structure coupling. *Brodogradnja*, 74(3), 145-164. https://doi.org/10.21278/brod74308

[11] Yao, H., Zhang, H., 2018. Numerical simulation of boundary-layer transition flow of a model propeller and the full-scale propeller for studying scale effects. *Journal of Marine Science and Technology*, 23(4), 1004-1018. https://doi.org/10.1007/s00773-018-0528-4

[12] Yao, H., Zhang, H., 2019. Improvements of scaling method recommended by ITTC at a lower reynolds number range. *Journal of Shanghai Jiaotong University*, 53(1), 35-41.

[13] Feng, D., Yu, J., He, R., Zhang, Z., Wang, X., 2020. Free running computations of KCS with different propulsion models. *Ocean Engineering*, 214, 107563. https://doi.org/10.1016/j.oceaneng.2020.107563

[14] Kok, Z., Duffy, J., Chai, S., Jin, Y., Javanmardi, M., 2020. Numerical investigation of scale effect in self-propelled container ship squat. *Applied Ocean Research*, 99, 102143. https://doi.org/10.1016/j.apor.2020.102143

[15] Yu, J., Yao, C., Liu, L., Zhang, Z., Feng, D.. 2021. Assessment of full-scale KCS free running simulation with body-force models. *Ocean Engineering*, 237, 109570. https://doi.org/10.1016/j.oceaneng.2021.109570

[16] Sun, W., Hu, S., Su, J., Wei, J., Huang, G., 2019. Numerical analysis of hull-propeller and free surface interaction at model- and full-scale. Sixth International Symposium on Marine Propulsors, 26-30 May, Rome, Italy.

[17] Sun, W., Hu, Q., Hu, S., Su, J., Xu, J., Wei, J., Huang, G., 2020. Numerical analysis of full-scale ship self-propulsion performance with direct comparison to statistical sea trail results. *Journal of Marine Science and Engineering*, 8(1), 24. https://doi.org/10.3390/jmse8010024

[18] Mikkelsen, H., Walther, J. H., 2020. Effect of roughness in full-scale validation of a CFD model of self-propelled ships. *Applied Ocean Research*, 99, 102162. https://doi.org/10.1016/j.apor.2020.102162

[19] Jasak, H., Vukčević, V., Gatin, I., Lalović, I. 2019., CFD validation and grid sensitivity studies of full scale ship self propulsion. *International Journal of Naval Architecture and Ocean Engineering*, 11(1), 33-43. https://doi.org/10.1016/j.ijnaoe.2017.12.004

[20] Saydam, A. Z., Küçüksu, G. N., İnsel, M., Gökçay, S., 2022. Uncertainty quantification of self-propulsion analyses with RANS-CFD and comparison with full-scale ship trials. *Brodogradnja*, 73(4), 107-129. https://doi.org/10.21278/brod73406

[21] Zhang, K., Li, Q., Zhang, J., Shi, H., Yu, J., Guo, X., Du, Y., 2022. Simulation and analysis of Back siltation in a navigation channel using MIKE 21. *Journal of Ocean University of China*, 21(4), 893-902. https://doi.org/10.1007/s11802-022-5052-9

[22] Berends, K., Scheel, F., Warmink, J., De Boer, W., Ranasinghe, R., Hulscher, S., 2019. Towards efficient uncertainty quantification with high-resolution morphodynamic models: A multifidelity approach applied to channel sedimentation. *Coastal engineering*, 152, 103520. https://doi.org/10.1016/j.coastaleng.2019.103520

[23] Li, C., Yang, Z., Chen, Y., 2019. Influence of Sediment Transport on Nangang Terminal at Shentou Harbor of Yangpu Port *Port Engineering Technology*, 56(5), 6-10. https://doi.org/10.16403/j.cnki.ggjs20190502

[24] Li, Y., Song, Z., Peng, G., Fang, X., Li, R., Chen, P., Hong, H., 2019. Modeling hydro-dynamics in a harbor area in the Daishan Island, China. *Water*, 11(2), 192. https://doi.org/10.3390/w11020192

[25] Lee, G.-H., Shin, H.-J., Kim, Y. T., Dellapenna, T. M., Kim, K. J., Williams, J., Kim, S.-Y., Figueroa, S. M., 2019. Field investigation of siltation at a tidal harbor: North Port of Incheon, Korea. *Ocean Dynamics*, 69, 1101-1120. https://doi.org/10.1007/s10236-019-01292-0

[26] Stern, F., Wilson, R. V., Coleman, H. W., Paterson, E. G., 2001. Comprehensive approach to verification and validation of CFD simulations-Part 1: methodology and procedures. *Journal of Fluids Engineering*, 123(4), 793-802. https://doi.org/10.1115/1.1412235

[27] Liu, L., Chen, M., Wang, X., Zhang, Z., Yu, J., Feng, D., 2021. CFD prediction of full-scale ship parametric roll in head wave. *Ocean Engineering*, 233, 109180. https://doi.org/10.1016/j.oceaneng.2021.109180

[28] Castro, A. M., Carrica, P. M., Stern, F., 2011. Full scale self-propulsion computations using discretized propeller for the KRISO container ship KCS. *Computers & Fluids*, 51(1), 35-47. https://doi.org/10.1016/j.compfluid.2011.07.005

[29] ITTC, 2014. Practical Guidelines for Ship CFD Applications. Available from: https://www.ittc.info/media/9773/75-03-02-03.pdf